Acta Oceanol. Sin., 2014, Vol. 33, No. 7, P. 65–71
DOI: 10.1007/s13131-014-0502-x
http://www.hyxb.org.cn
E-mail: hyxbe@263.net

A model of sea surface temperature front detection based on a threshold interval

PING Bo[1,2,3], SU Fenzhen[2,3]*, MENG Yunshan[2], FANG Shenghui[1], DU Yunyan[2]

[1] School of Remote Sensing and Information Engineering, Wuhan University, Wuhan 430079, China
[2] Laboratory of Resources and Environmental Information System, Institute of Geographic Sciences and Natural Resources Research, Chinese Academy of Sciences, Beijing 100101, China
[3] Collaborative Innovation Center of South China Sea Studies, Nanjing 210093, China

Received 26 April 2013; accepted 11 November 2013

Abstract

A model (Bayesian oceanic front detection, BOFD) of sea surface temperature (SST) front detection in satellite-derived SST images based on a threshold interval is presented, to be used in different applications such as climatic and environmental studies or fisheries. The model first computes the SST gradient by using a Sobel algorithm template. On the basis of the gradient value, the threshold interval is determined by a gradient cumulative histogram. According to this threshold interval, front candidates can be acquired and prior probability and likelihood can be calculated. Whether or not the candidates are front points can be determined by using the Bayesian decision theory. The model is evaluated on the Advanced Very High-Resolution Radiometer images of part of the Kuroshio front region. Results are compared with those obtained by using several SST front detection methods proposed in the literature. This comparison shows that the BOFD not only suppresses noise and small-scale fronts, but also retains continuous fronts.

Key words: sea surface temperature, threshold setting, Sobel algorithm, edge detection, front detection

Citation: Ping Bo, Su Fenzhen, Meng Yunshan, Fang Shenghui, Du Yunyan. 2014. A model of sea surface temperature front detection based on a threshold interval. Acta Oceanologica Sinica, 33(7): 65–71, doi: 10.1007/s13131-014-0502-x

1 Introduction

An oceanic front is a narrow zone of enhanced horizontal gradients of water properties (temperature, salinity, nutrients, and others) that separates broader areas with different water masses or different vertical structures (stratification) (Belkin et al., 2009). A sea surface temperature (SST) front is a type of oceanic front that plays a crucial role in oceanography and marine ecology. SST fronts and their association with currents are important in heat transport and ecosystem functioning.

In the past decades, many methods have been applied to producing clear views of SST fronts. The SST fronts in the western Pacific Ocean have been studied by taking advantage of the wide-area observation of remote sensing data, available since the 1980s (Huh, 1982). Cayula and Cornillon (1992, 1995) developed a complex histogram-based method to detect fronts near North Carolina in satellite SST images, which operates at three levels-picture, window, and local/pixel levels. Diehl et al. (2001) improved this method via an unfixed size window for histogram computation; the window size is determined by semivariance. These methods can detect clouds and remove them automatically. The foregoing two front detection algorithms are both based on the condition that the temperature histogram in each window is unimodal, and use unsupervised learning methods and statistical decision-making on the existence of a front. The edge contour is ultimately completed by a region-based algorithm. Though these methods are proven for front detection, they are affected by impulsive noise, in which case prior median filtering is needed. This filtering may smooth some significant information that cannot be detected afterward. In addition, some steps require a threshold for detection. The threshold setting is subjective in certain circumstances, and demands numerous experiments for its determination.

Vázquez et al. (1999) developed an entropic approach to edge detection for SST images. It consists mainly of two steps-edge detection using Jensen-Shannon divergence, and edge linking. Shimada et al. (2005) improved this method by implementation of mathematical morphology instead of edge linking. The two algorithms need to set a threshold that is used to determine the edge. The threshold setting for these algorithms is single and subjective, and often requires numerous experiments for its determination.

Some classic edge detection algorithms are also designed for oceanographic applications. For example, intensity gradient detectors (Sobel, Prewitt, Kirsch and others) are used in oceanographic texture analysis (Sauter and Parson, 1994) and in automatic detection of Gulf Stream rings (Janowitz, 1985). Second-derivative techniques (e.g., the Laplacian or Laplacian of Gaussian) are used in fish detection (Savage et al., 1994). After the gradient computation step in traditional edge detection algorithms, a threshold is set. By comparing the gradient value with the threshold, oceanic fronts can be detected. If the gradient value of a pixel is larger than the threshold, then it is considered as a front point; otherwise, it is classified as a non-front point. Based on the analysis above, these methods are strongly dependent on the threshold, and its setting is seriously affected by subjectivity. If the threshold is large, noise is reduced but

Foundation item: The National Key Technology R&D Program of China under contract No. 2011BAH23B04; the National High Technology Research and Development Program (863 Program) of China under contract No. 2007AA092202.
*Corresponding author, E-mail: sufz@lreis.ac.cn

fronts may be filtered out; if it is small, frontal information can be extracted, but results will be mixed with substantial noise.

In certain cases for a single front, a perfect threshold does not exist. For example, an ideal front is designed by separating two different temperature water masses (Fig. 1). In Region A, assume the gradient value of the front is 0.8, and in Region B it is 0.4. Undoubtedly, when the threshold is set to 0.4, the entire front can be detected. Near Region A, however, there may be so much noise that it reduces the accuracy of front detection. But when the threshold is set to 0.8, the front near Region B may be filtered. So, for this type of front, a single threshold is not adequate for detection.

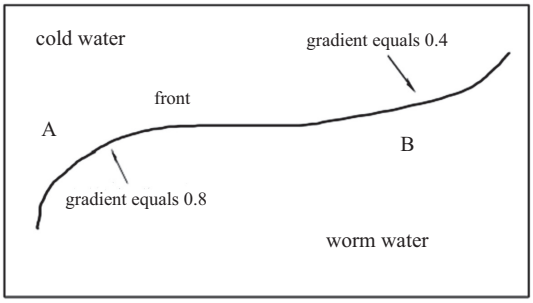

Fig.1. Illustration of nonexistence of an ideal front designed to illuminate a single threshold.

To solve the problems presented by a single threshold, we set a threshold interval to partially eliminate reliance on threshold setting. In contrast with the single threshold setting that demands numerous experiments and significant expertise, the threshold interval only requires setting of approximate upper and lower thresholds. Subjectivity in the experiments can thus be reduced.

The Canny operator (Canny, 1986) was proposed with the goal of finding an optimal algorithm satisfying three norms: (1) good signal to noise ratio; (2) good location; and (3) one response for one edge. This operator is widely used in edge and front detections. Oram et al. (2008) used Canny operator to detect fronts in the southern California Bight. The algorithm can remove clouds and be used for the mesoscale front detection. Shi et al. (2010) integrated the Canny and mathematical morphology algorithms for the front detection in the South China Sea. This approach first uses Canny method for initial front detection, and then the front is thinned and linked via the mathematical morphology algorithm. Because Canny method is based on a threshold interval for edge detection, it is similar to the Bayesian oceanic front detection (BOFD) model. Hence, the Canny method is used for comparison with the BOFD. Similar to the BOFD, Zhang et al. (2007) applied the Bayesian Statistical Inference (BSI) for edge detection. The difference between the BSI and the BOFD is that the BSI is based on sample data to estimate prior probability and likelihood; the BOFD does not need to do these.

We have structured the remainder of the paper as follows. The BOFD model is introduced in Section 2. Section 3 describes SST data used and experiments based on the BOFD model. Conclusions are presented in Section 4.

2 BOFD model

The BOFD model is proposed for oceanic front detection, based on the Bayesian decision theory. This section mainly consists of seven parts, including introduction of the Bayesian decision theory, gradient computation, prior probability calculation, local degree of edge, block deviation computation, likelihood computation, and algorithm flow-chart.

2.1 *Bayesian decision theory*

The Bayesian decision theory is a quantitative compromise between the use of probabilities of different classification decision-making and corresponding decision cost (Duda et al., 2003). Here, all image pixels are separated into two classifications: front (ω_i denotes the front classification) and non-front (ω_j is the non-front classification). Providing that the prior probability that a pixel (A designates this pixel) belongs to the front classification is already known, i.e., $P_{\mathrm{A}}(\omega_i)$, then the prior probability that the pixel belongs to the non-front classification is $1-P_{\mathrm{A}}(\omega_i)$, or $P_{\mathrm{A}}(\omega_j)$.

If a pixel (A denotes this pixel) belongs to the front classification, the probability that another A's feature x appears is $P_{\mathrm{A}}(x|\omega_i)$; similarly, if A belongs to the non-front classification, the probability that the same feature x appears is $P_{\mathrm{A}}(x|\omega_j)$. If $P_{\mathrm{A}}(\omega_i)$, $P_{\mathrm{A}}(\omega_j)$, $P_{\mathrm{A}}(x|\omega_i)$ and $P_{\mathrm{A}}(x|\omega_j)$ can all be acquired, based on the Bayesian theory, $P_{\mathrm{A}}(\omega_i|x)$ and $P_{\mathrm{A}}(\omega_j|x)$ can be calculated with the following equation:

$$\left.\begin{aligned} P_{\mathrm{A}}(\omega_i \mid x) &= \frac{P_{\mathrm{A}}(x \mid \omega_i) P_{\mathrm{A}}(\omega_i)}{P_{\mathrm{A}}(x)} \\ P_{\mathrm{A}}(\omega_j \mid x) &= \frac{P_{\mathrm{A}}(x \mid \omega_j) P_{\mathrm{A}}(\omega_j)}{P_{\mathrm{A}}(x)} \end{aligned}\right\}. \tag{1}$$

$P_{\mathrm{A}}(\omega_i|x)$ and $P_{\mathrm{A}}(\omega_j|x)$ are termed posterior probability that Pixel A belongs to ω_i and ω_j under the circumstance that feature x is known. Owing to only two classifications (front and non-front) are used, $P_{\mathrm{A}}(x)$ can be expressed as follows:

$$P_{\mathrm{A}}(x) = \sum_{p=1}^{2} P(x \mid \omega_p) P(\omega_p) . \tag{2}$$

Equation (1) indicates that with use of the value of feature x, a prior probability $P(\omega_i)$ can be converted to the posterior probability $P(\omega_i \mid x)$, as with $P(\omega_j \mid x)$. In other words, assuming that the feature value x is known, Eq. (1) can determine the probability that Pixel A belongs to ω_i. Similarly, the probability that A belongs to ω_j can be acquired. In Eq. (1), the scalar factor $P_{\mathrm{A}}(x)$ is not important for making certain determinations, so we remove this factor. Finally, equivalent decision rules can be expressed as follows:

$$\theta \in \left\{ \begin{aligned} &\omega_i, P_{\mathrm{A}}(x \mid \omega_i) P_{\mathrm{A}}(\omega_i) > P_{\mathrm{A}}(x \mid \omega_j) P_{\mathrm{A}}(\omega_j) \\ &\omega_j, P_{\mathrm{A}}(x \mid \omega_i) P_{\mathrm{A}}(\omega_i) < P_{\mathrm{A}}(x \mid \omega_j) P_{\mathrm{A}}(\omega_j) \end{aligned} \right\}. \tag{3}$$

So, if $P_{\mathrm{A}}(x \mid \omega_i) P_{\mathrm{A}}(\omega_i) > P_{\mathrm{A}}(x \mid \omega_j) P_{\mathrm{A}}(\omega_j)$, then A is a front point; if not, A is a non-front point.

2.2 *Gradient computation*

Currently, most methods of gradient computation are based on a template, using convolution to compute the central pixel

gradient. The Sobel algorithm operator is popular, owing to its simplicity and rapid gradient calculation. It is widely applied to gradient calculation, edge detection, oceanic front detection and others. It has achieved favorable results. The gradient computation here is based on the Sobel algorithm operator. Its template can be expressed as Fig. 2.

−1	−2	−1
0	0	0
1	2	1

−1	0	1
−2	0	2
−1	0	1

Fig.2. Sobel algorithm operator.

The convolution computation is done on each image pixel to obtain the first-order derivatives $Grad\_T_x$ and $Grad\_T_y$ in the x and y directions, respectively. For each pixel, a 3×3 square neighborhood is expressed as in Fig. 3. In this figure, E designates the central pixel.

A	B	C
D	E	F
G	H	I

Fig.3. 3×3 neighborhood for each pixel.

Then, $Grad\_T_x$ and $Grad\_T_y$ for E can be expressed as

$$\left.\begin{aligned} Grad\_T_x &= T_{\mathrm{G}} + 2T_{\mathrm{H}} + T_{\mathrm{I}} - T_{\mathrm{A}} - 2T_{\mathrm{B}} - T_{\mathrm{C}} \\ Grad\_T_y &= T_{\mathrm{C}} + 2T_{\mathrm{F}} + T_{\mathrm{I}} - T_{\mathrm{A}} - 2T_{\mathrm{D}} - T_{\mathrm{G}} \end{aligned}\right\}, \tag{4}$$

where T_{A} is the temperature of Pixel A. So, the temperature gradient for E is calculated by

$$Grad\_T_{\mathrm{E}} = (Grad\_T_x^2 + Grad\_T_y^2)^{\frac{1}{2}}. \tag{5}$$

A gradient image can be acquired by calculating the gradient for each pixel using the methods above.

2.3 *Threshold interval setting*

The threshold interval is set according to the gradient image. If a pixel's gradient value is larger than the upper threshold, it is considered as a front point; if its gradient value is smaller than the lower threshold, it is designated as a non-front point. If the gradient value is between the upper and lower thresholds, the pixel is considered as a front candidate. Based on the threshold interval, we calculate the prior probability and likelihood for every candidate. Compared with the single threshold, the threshold interval can partially eliminate subjectivity in threshold setting.

The method of setting the threshold interval is very important here for front detection accuracy. So, based on the Canny edge algorithm and a series of applications (Oram et al., 2008; Rivas and Pisoni, 2009), the gradient cumulative histogram is used to set the upper and lower thresholds. Noise approximately accords with a Gaussian distribution in the gradient cumulative histogram; however, edge points are almost composed of large gradient-value pixels and edges account for a relatively low proportion of all pixels. Hence, according to Oram et al. (2008), the upper and lower thersholds are defined at 0.9 and 0.8 of cumulative histogram,respectively. Actually, this threshold interval setting is a subjective task. And the authors have verified the fact that even if the upper threshold is chosen at 0.95 of cumulative histogram and the lower threshold is chosen at 0.7 or even at 0.6 of cumulative histogram, the differences between the results are not very obvious. This fact also verifies that the BOFD method can reduce the subjectivity of threshold setting. Figure 4a shows such a cumulative histogram constructed from the gradient image of experimental area mentioned in Section 3.1, and Fig. 4b shows the local enlarged image of the cumulative histogram, with the upper and lower thresholds defined at 0.9 and 0.8, respectively.

2.4 *Prior probability calculation*

On the basis of threshold interval, whether a front candidate is a front point is represented by a probability distribution. This probability can be considered as the prior probability. The prior probability of Pixel A is a front pixel can be computed by

$$P_{\mathrm{A}}(\omega_i) = \frac{Grad\_T_{\mathrm{A}} - u_l}{u_u - u_l}, \tag{6}$$

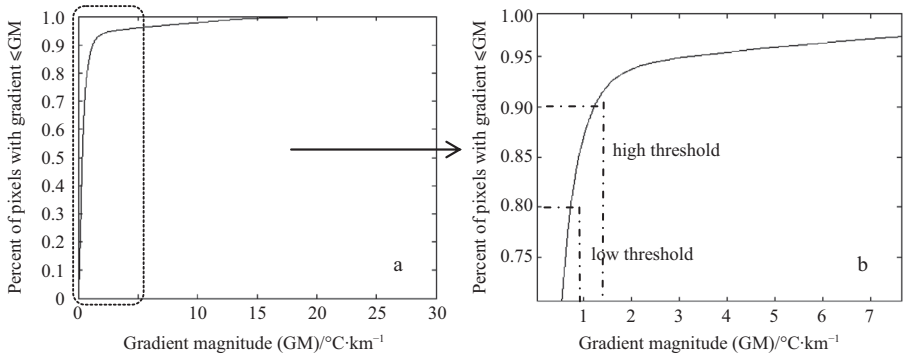

Fig.4. Gradient cumulative histogram (a) and local enlarged image of the cumulative histogram (b).

where $Grad\_T_A$ is Pixel A's gradient value, and u_l and u_u are the lower and upper thresholds, respectively. Similarly, the prior probability of Pixel A is non-front pixel can be computed by

$$P_A(\omega_j) = \frac{u_u - Grad\_T_A}{u_u - u_l}. \quad (7)$$

Take the threshold interval between 20 and 100 as an example. If a front candidate gradient value is 80, the probability that it is classified as a front point is (80–20)/(100–20), or about 75%. Similarly, there is about 25% probability of classification as a non-front point.

2.5 *Local degree of edge and block deviation*

Based on Fig. 3., the larger the difference is between two diagonal pixels (A and I, or C and G), between two horizontal pixels(D and F), or between two vertical pixels(B and H), the greater the likelihood that the central pixel is a front point (Mansoori and Eghbali, 2006). For each pixel, a 3×3 square neighborhood is selected to compute the local degree of edge (LDE) and block deviation (BD). Vector $\vec{v}$ =[A, B, C, D, F, G, H, I] represents the neighborhood pixels (Fig. 3 shows a 3×3 square neighborhood which the central point is E), V_{max} represents the largest value of $\vec{v}$, V_{min} represents the smallest value of $\vec{v}$, and $\bar{V}$ represents the mean value of $\vec{v}$. So, take diagonal points A and I as an example, the LDE and the BD can be calculated by the following equation:

$$\left.\begin{aligned} D_{lde}(A,I) &= (4/7)\times\frac{V_{max} - \bar{V} - |T_A - T_I|}{V_{max} - V_{min}} + (1/2) \\ D_{bd}(A,I) &= \frac{|T_A - T_I|}{V_{max} - V_{min}} \end{aligned}\right\}, \quad (8)$$

where D_{lde}(A,I) and D_{bd}(A,I) are the LDE and the BD for pixels A and I, respectively. Then, for the central pixel E, the LDE and the BD can be computed by

$$\begin{aligned} D_{lde}(E) &= \frac{1}{4}\times[D_{lde}(A,I) + D_{lde}(B,H) + D_{lde}(C,G) + D_{lde}(D,F)], \\ D_{bd}(E) &= \frac{1}{4}\times[D_{bd}(A,I) + D_{bd}(B,H) + D_{bd}(C,G) + D_{bd}(D,F)], \end{aligned} \quad (9)$$

where D_{lde}(E) is the local degree of edge of central pixel E; and D_{bd}(E) is its block deviation. The LDE and the BD for each pixel are computed using Eq. (9), and their ranges are between 0 and 1.

2.6 *Likelihood computation*

The likelihood of *M* given *N*, also called conditional probability, is the probability of *M* if *N* is known to occur or has occurred. Here, *M* represents the LDE and the BD for each candidate, and *N* indicates the classification to which a candidate belongs (front or non-front).

If candidate X is considered as a front point, then candidates with gradient value larger or equal to that of X may also be considered as front points. These candidates compose a set, called the front-set. Similarly, if X is considered as a non-front point, then candidates with gradient value smaller or equal to that of X can be considered as non-front points. These candidates compose the non-front-set. The number of differences between front-set candidates' LED and BD and X's LED and BD less than 0.1 are counted, respectively, and designated m_1 and m_2. The number of front-set can also be acquired, called *n*. We calculate the proportion of m_1 and *n*, and m_2 and *n*. The two ratios are approximate conditional probabilities of two features (LED and BD) in the case where X is considered as a front point. In such a case, this is the likelihood of these two features, which can be expressed as $P(X_a|\omega_i)$, where *a* represents LED and BD, and ω_i stands for the front point. Similarly, when X is considered as non-front, two approximate conditional probabilities can be attained and expressed as $P(X_a|\omega_j)$, where ω_j stands for a non-front point.

Based on the threshold interval, we can obtain four conditional probabilities for each candidate. To achieve high computational efficiency, a naive Bayesian model expressed as the following equation is applied to computing comprehensive likelihood:

$$P(q|\omega_k) = \prod_{a=1}^{2} P(X_a|\omega_k), \; k=1,2. \quad (10)$$

On the basis of the prior probability and the likelihood, whether a candidate is a front point can be verified by Eq. (3).

2.7 *Algorithm flowchart*

The entire algorithm flow-chart can be described.

(1) For one SST data point, gradient values, LDE, and BD are acquired using the aforementioned methods.

(2) Based on the gradient cumulative histogram, upper and lower thresholds are defined. Pixels whose gradient values are smaller than the lower threshold are considered as non-front points; pixels with gradient values larger than the upper threshold are considered as front points; pixels with gradient values between upper and lower thresholds are considered as frontal candidates. For each candidate point, the prior probability can be calculated based on the threshold interval using Eqs (6) and Eq. (7), and likelihood can be computed using Eq. (10).

(3) Based on the prior probability and the comprehensive likelihood, the posterior probability can be computed and the front detection can be achieved by using Eq. (3).

The algorithm flow-chart is presented in Fig. 5.

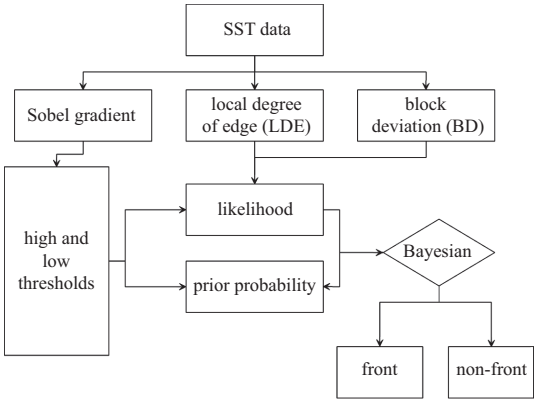

Fig.5. Algorithm flow-chart.

3 Data and experiments

3.1 *Data introduction*

The SST data are used to verify the validity of the algorithm. The SST data are derived from National Oceanographic and Atmospheric Administration (NOAA; NOAA-11) Advanced Very High Resolution Radiometer (AVHRR) SST images, with resolution of about 4 km. Cloud-contaminated pixels can be determined as frontal pixels during front detection, so cloud-free images are necessary for the algorithm. The monthly mean map of May 2007a is used to test the algorithm, because of its cloud-free conditions and clarity of fronts. The data for the study area (23°66′–34°65′N, 123°20′–140°78′E) was first extracted from raw data. Figure 6 shows the image for the study area. The range of raw data in the area is from 0 to 436. Since the land temperature is not calculated, based on Eq. (11), the area oceanic temperature is from 0°C to 29.7°C.

$$T_a=0.075d_I-3, \tag{11}$$

where T_a is actual oceanic temperature; d_I is the index data value acquired from the raw data.

3.2 *Results from BOFD and Sobel*

The threshold interval is defined by the cumulative histogram which is shown as Fig. 4. The upper and lower thresholds are defined at 0.9 and 0.8 of the cumulative histogram and the specific threshold values for the experimental area are 1.23 and 0.738 °C/km, respectively. In addition, the upper and lower thresholds are also defined by using the same method in the single threshold Sobel algorithm, the single Kirsch algorithm and Canny algorithm. Figure 7a is the result of front detection from the BOFD model; Fig. 7b is the result from Sobel algorithm with the lower threshold; Fig. 7c is the result from Sobel algorithm with the upper threshold.

In Fig. 7b, there is a considerable noise and many small edges (indicated by white arrows), and the edge detection accuracy is low. In Fig. 7c, although the noise is reduced in some places, some frontal segments are lost, causing fronts to be discontinuous (designated by white arrows). Relative to Sobel algorithm with only one threshold, the result of BOFD algorithm suppresses the noise and improves the accuracy of edge detection.

3.3 *Results of BOFD and other front detection methods*

We compare the BOFD model with other front detection methods, including Kirsch, Laplacian, Canny, and Jensen-Shannon divergence. The Kirsch method is selected for its simplicity, and is widely applied to edge detection. The Laplacian method is isotropic and independent of direction; it also achieves some successful outcomes in edge detection. Canny method has long been considered as an effective method for front and edge detection. It also uses upper and lower thresholds for detection, similar to the BOFD, so is selected for comparison. Jensen-Shannon divergence has also been used in front detection (Vázquez et al., 1999; Shimada et al., 2005).

First, the threshold interval setting is based on the cumulative histogram. The upper and lower thresholds for both Kirsch and Canny methods are also selected by the gradient cumulative histogram, at 0.9 and 0.8, respectively. Figure 8 shows the results from the BOFD and other edge detection methods: Fig. 8a is the BOFD result; Fig. 8b is from Kirsch method with the lower threshold; Fig. 8c is from Kirsch method with the upper threshold; Fig. 8d is from Jensen-Shannon divergence; Fig. 8e is from Canny method; Fig. 8f is from the Laplacian method. The Laplacian and Canny methods are first Gaussian-filtered, which is defined by the following equation, with $\sigma = 2$:

$$G=\exp\frac{-x^2-y^2}{2\sigma^2},\ F_x=\frac{\partial G}{\partial x},\ F_y=\frac{\partial G}{\partial y}. \tag{12}$$

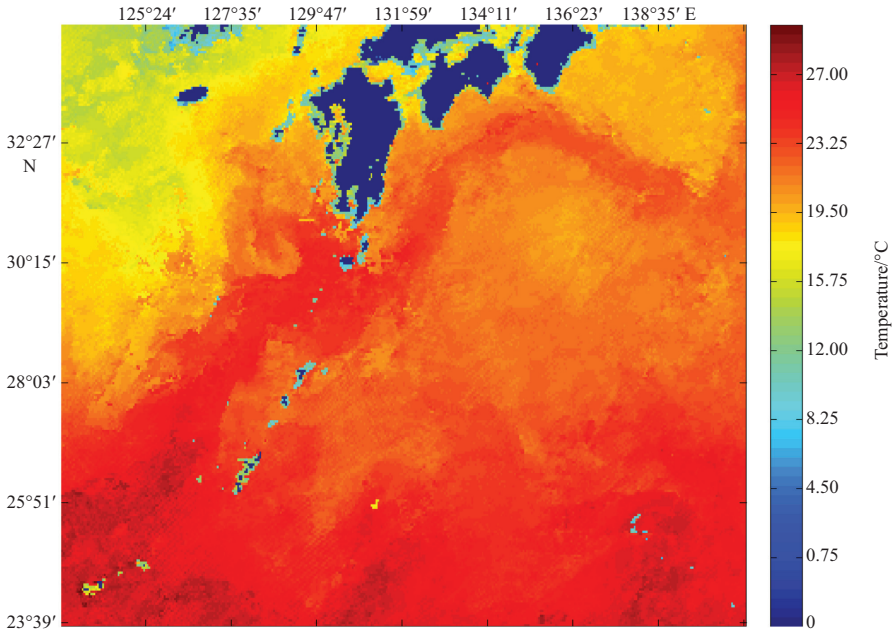

Fig.6. Geographic situation of study area.

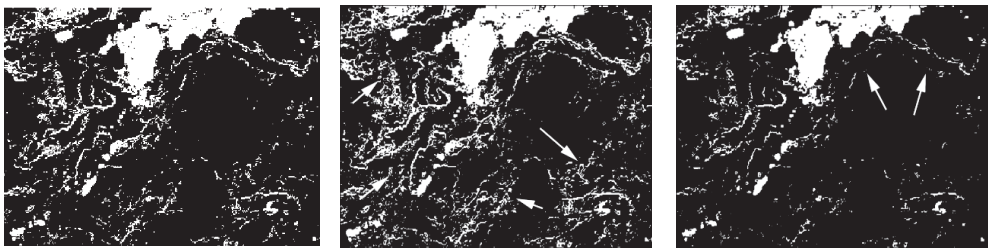

(a) (b) (c)

Fig.7. Comparison between BOFD with upper and lower thresholds and Sobel algorithm with only one threshold and result from BOFD (a), Sobel with lower threshold (b) and Sobel with upper threshold (c)

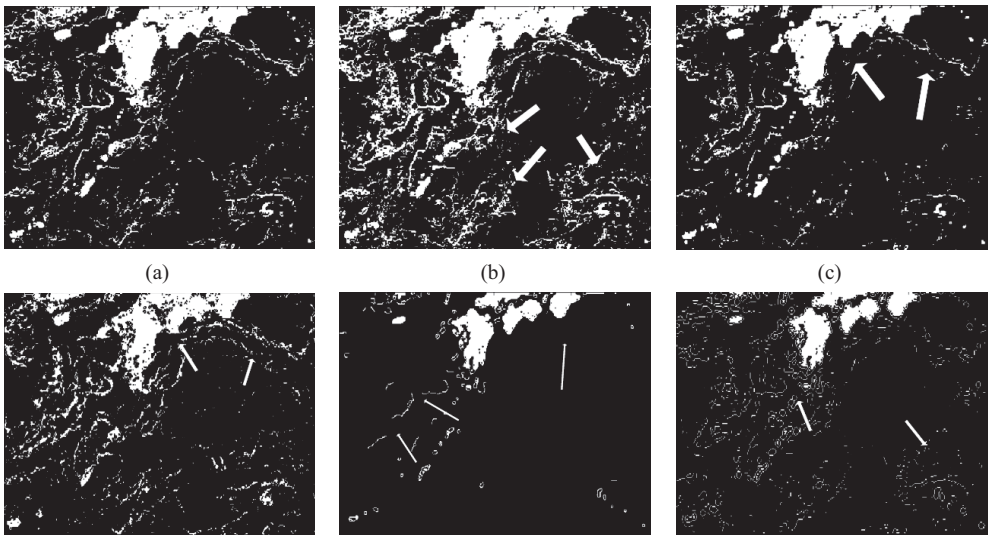

(a) (b) (c)

(d) (e) (f)

Fig.8. Comparison between BOFD and other front detection methods. Results from BOFD (a), Kirsch with lower threshold (b), Kirsch with upper threshold (c), Jensen-Shannon divergence (d), Canny with upper and lower thresholds (e) and Laplacian (f).

Front detection with Kirsch method has the same problems as single-threshold Sobel algorithm. When the threshold is lower, some noise and small fronts are detected (shown by white arrows in Fig. 8b). When the threshold is higher, the detected fronts are discontinuous (shown by white arrows in Fig. 8c). Precise threshold setting requires numerous experiments.

Jensen-Shannon divergence front detection is useful, but some noise and small-scale fronts are retained and some fronts are discontinuous (indicated by white arrows in Fig. 8d). Again, a single threshold setting is easily affected by subjectivity.

The Gaussian filter helps Canny method remove some noise and small-scale fronts, and edge thinning helps position fronts precisely. However, some fronts are filtered or discontinuous (indicated by white arrows in Fig. 8e), despite a threshold interval setting identical to that of the BOFD.

Owing to the Gaussian filter, the Laplacian method somewhat reduces noise. There is a dual-edge problem, however, and noise can be increased (designated by white arrows in Fig. 8f). Further, edge positioning precision is poor with the Laplacian method.

4 Conclusions

In this paper, front detection based on the threshold interval was presented. Compared with some classic edge detection methods, the BOFD does not require setting of a precise threshold.

The result of BOFD with the threshold interval is noise and small-scale front suppression, and it is suitable for preserving some front information. Single-threshold Sobel and Kirsch techniques are not as effective as the BOFD, because they both rely heavily on threshold setting, and this setting frequently necessitates numerous experiments. Canny method is similar to the BOFD, but its threshold interval usage differs from the BOFD. The Canny threshold interval is for direct edge detection, whereas that of the BOFD is used for determining front candidates. Compared with Canny method, the BOFD is less reliant on threshold setting. Jensen-Shannon divergence front detection is useful, but like Sobel algorithm and Kirsch method, the algorithm depends on the threshold setting.

Although the BOFD partially eliminates reliance on the threshold setting, its threshold interval setting is also somewhat

subjective. Attainment of a precise threshold interval is important within the BOFD model, so this must be a focus of future work.

Acknowledgements

The authors would like to thank Wuhan University and Institute of Geographic Sciences and Natural Resources Research for the support.

References

Belkin I, Cornillon P, Sherman K. 2009. Fronts in large marine ecosystems. Progress in Oceanography, 81: 223–236

Canny J. 1986. A computational approach to edge detection. IEEE Transactions Pattern Analysis and Machine Intelligence PAMI, 8(6): 679–698

Cayula J F, Cornillon P. 1992. Edge detection algorithm for SST images. Journal of Atmospheric and Oceanic Technology, 9: 67–80

Cayula J F, Cornillon P. 1995. Multi-image edge detection for SST images. Journal of Atmospheric and Oceanic Technology, 12: 821–829

Diehl F, Budd W, Ullman D, et al. 2001. Geographic window sizes applied to remote sensing sea surface temperature front detection. Journal of Atmospheric and Oceanic Technology, 19: 1105–1113

Duda R, Hart P, Stock D. 2003. Pattern Classification (in Chinese). Beijing: China Ocean Press, 16–18

Huh O K. 1982. Satellite observations and the annual cycle of surface circulation in the Yellow Sea, East China Sea, and Korea Strait. La Mer, 20: 210–222

Janowitz M F. 1985. Automatic Detection of Gulf Stream Rings. MASSACHUSETTS UNIV AMHERST, No. TR-J850

Mansoori E, Eghbali H. 2006. Heuristic edge detection using fuzzy rule-based classifier. Journal of Intelligent and Fuzzy Systems, 17: 457–469

Oram J, Mcwilliams J, Stolzenbach K. 2008. Gradient-based edge detection and feature classification of sea-surface images of the southern California Bight. Remote Sensing of Environment, 112(5): 2397–2415

Rivas A, Pisoni J. 2009. Identification, characteristics and seasonal evolution of surface thermal fronts in the Argentinean continental shelf. Journal of Marine Systems, 79: 134–143

Sauter D, Parson L. 1994. Spatial filtering for speckle reduction contrast enhancement, and texture analysis of GLORIA images. IEEE J Oceanic Eng, 19: 563–576

Savage C R, Petrell R J, Neufeld T P. 1994. Underwater fish video images: image quality and edge detection techniques. Can Agric End, 36: 175–183

Shimada T, Sakaida F, Kawamura H, et al. 2005. Application of an edge detection method to satellite images for distinguishing sea surface temperature fronts near the Japanese coast. Remote Sensing of Environment, 98(1): 21–34

Shi Hanqing, Zhang Wei, Yin Zhiquan. 2010. Study on ocean front detection based on Canny operator and mathematical morphology. International Conference on Remote Sensing (in Chinese). China: China Academic Journal Electronic Publishing House, 4: 252–255

Vázquez D P, Chakir Atae-Allah, Pedro L L.1999. Entropic approach to edge detection for SST images. Journal of Atmospheric and Oceanic Technology, 16: 970–979

Zhang Hao, Cai Jinhui, Huang Pingjie, et al. 2007. Edge detection of complex scenes based on Bayesian statistical inference. Journal of South China University of Technology: Natural Science Edition (in Chinese), 35(9): 40–44